Oxygen consumption of cell suspension in a poly(dimethylsiloxane) (PDMS) microchannel estimated by scanning electrochemical microscopy

Takeshi Saito,[a] Ching-Chou Wu,[b] Hitoshi Shiku,*[a] Tomoyuki Yasukawa,[a] Masaki Yokoo,[c] Takashi Ito-Sasaki,[c] Hiroyuki Abe,[c] Hiroyoshi Hoshi[d] and Tomokazu Matsue*[ac]

Received 4th January 2006, Accepted 17th July 2006
First published as an Advance Article on the web 3rd August 2006
DOI: 10.1039/b600080k

A quantitative analysis of the oxygen concentration profile near a poly(dimethylsiloxane) (PDMS) microfluidic device was performed using scanning electrochemical microscopy (SECM). A microchannel filled with sodium sulfite (Na_2SO_3) aqueous solution was imaged by SECM, showing that the oxygen diffusion layer of the PDMS microchannel was observed to be hemicylindrical. Based on a theoretical analysis of the hemicylindrical diffusion layer of the microchannel, the total oxygen mass transfer rates of oxygen to the PDMS microchannel filled with the Na_2SO_3 solution was calculated to be $(4.01 \pm 0.30) \times 10^{-12}$ mol s^{-1}. This is the maximum value of the oxygen transfer rate for this PDMS microchannel device. The oxygen consumption rate increased almost linearly with the logarithm of the concentration of *E. coli* cells ($10^6 \sim 10^8$ cells). The respiratory activity for a single *E. coli* cell was estimated to be $\sim 4.31 \times 10^{-20}$ mol s^{-1} $cell^{-1}$.

1. Introduction

Microfluidic devices fabricated by soft lithography using poly(dimethylsiloxane) (PDMS) have become a central tool in a number of miniaturized micro-total analysis systems (μ-TAS);[1–4] further, they have been applied in various analytical fields of chemistry, biology, and biomedical studies. In particular, patterning, characterization and manipulation of various kinds of cells are the promising, practical applications of PDMS microchannel devices[5–7] because of the non-toxicity of the PDMS material. Culture systems utilizing PDMS microchannels for mammalian embryos were introduced by Beebe *et al.* to demonstrate a series of cultivation operations *in vitro*.[8,9] Diluzio *et al.* reported that a specific swarming movement of *Escherichia coli* (*E. coli*) occurred along the PDMS microchannel.[10] Cho *et al.* and Horsman *et al.* developed a cell sorter device for motile human sperm.[11,12] Takayama *et al.* used a multiple laminar flow system to create cellular patterns and locally deliver chemical reagents within a microchannel.[13]

Although many applications of PDMS microchannel for biological samples have been proposed, quantitative information on cell viabilities within such microchannels is limited.[14,15] Therefore, it is necessary to develop methods to simply evaluate the activity of biological samples applicable for the microchannel system. As one of the techniques to elucidate complex metabolic processes, scanning electrochemical microscopy (SECM) has been used to quantitatively analyze the mass transfer in a localized chemical reaction under physiological conditions.[16] Localized 2D or 3D concentration profiles were analyzed by SECM to determine the mass transfer rates to and from the surface of various samples,[17–20] including *E. coli* cells,[21,22] mammalian cells,[23–26] and embryos.[27–31]

In this paper, the oxygen concentration profiles near the PDMS and SU-8 microchannels were visualized with SECM. The oxygen diffusion layer formed along the microchannel was found to be hemicylindrical. This is the first study to report direct imaging of the hemicylindrical diffusion layers, although it is well known that such cylindrical diffusion layers are formed at the microband electrodes[32–35] or reaction zones with a channel-like shape. The measuring and analyzing procedures we introduced here combine the PDMS microchannel with SECM, and will be helpful to continuously operate and characterize various cell suspensions; they are also applicable in microfluidic systems to sequentially operate sample solutions and control measuring conditions.

2. Experimental

2.1 Chemicals

Special grade reagents of D-(+)-glucose, potassium chloride (KCl), potassium hexacyanoferrate (II) trihydrate, ($K_4Fe(CN)_6 \cdot 3H_2O$), potassium dihydrogenphosphate (KH_2PO_4), sodium chloride (NaCl), disodium hydrogenphosphate 12-water ($Na_2HPO_4 \cdot 12H_2O$), sodium dihydrogenphosphate (NaH_2PO_4), sodium nitrite ($NaNO_3$) and sodium sulfite (Na_2SO_3) were purchased from Wako Pure Chemical Industries, Ltd, Japan and used without further purification.

[a]*Graduate School of Environmental Studies, Tohoku University, 6-6-11-604 Aramaki, Aoba-ku, Sendai, 980-8579, Japan. E-mail: matsue@bioinfo.che.tohoku.ac.jp; shiku@bioinfo.che.tohoku.ac.jp; Fax: +81-22-795-7209; Tel: +81-22-795-7281*
[b]*Department of Bio-industrial Mechatronics Engineering, Chung Hsing University, Taichung, Taiwan*
[c]*Tohoku University Biomedical Engineering Research Organization (TUBERO), 2-1 Seiryo, Aoba-ku, Sendai, 980-8575, Japan*
[d]*Research Institute for the Functional Peptides, 4-3-32 Shimojo, Yamagata, 990-0823, Japan*

All the solutions were prepared using the distilled water obtained from a Milli-Q (Millipore, Japan).

2.2 Fabrication of microchannel device

A microchannel device was fabricated with PDMS (Silpot 184W/C, Dow Corning, USA) and bonded to a 60 mm plastic dish as shown in Fig. 1(a). The fabrication procedure is described elsewhere.[36] Briefly, a PDMS microchannel on a slide glass was replicated from an SU-8 mold (SU-8 2100, MicroChem Corp., USA) by using soft-lithography techniques. The replicated PDMS microchannel with a width of 200 μm, a depth of 220 μm and a length of 15 000 μm (practical channel volume, 660 nL; total volume of the fluidic device part, 920 nL) and a PDMS membrane with a thickness of 7 μm was bonded by using O_2 plasma treatment at 100 W for 15 s. A sample solution was dropped on the inlet and introduced into the microchannel by using a microsyringe connected at the outlet of the device (Fig. 1 (b)). An SU-8 microchannel device with an identical geometrical design was similarly microfabricated.

2.3 SECM measurement

The Pt microelectrode for the SECM experiment was fabricated as previously reported.[37] Briefly, a Pt wire with a diameter of 20 μm was electrochemically etched in a saturated $NaNO_3$ solution at room temperature, inserted into a soft-glass capillary (PG101654, World Precision Instruments, USA), and fused at 320 °C to cover the etched Pt wire with the glass. The tip radius was determined by cyclic voltammetry in a 4.0 mM $K_4Fe(CN)_6{\cdot}3H_2O$, 0.1 M KCl solution. Electrodes with tip radii of 1–2 μm were selected and used for the measurements. The radius, including the part sealed by glass, was smaller than 10 μm. The measurement was carried out in PBS solution (100 mM KCl, 25 mM $Na_2HPO_4{\cdot}12H_2O$ and 25 mM NaH_2PO_4) at room temperature, with a two-electrode configuration using an Ag/AgCl electrode as the reference electrode. The oxygen reduction currents at −0.50 V *versus* Ag/AgCl was amplified with a current amplifier (428MS, Keithley). The microelectrode tip was located at the center of the microchannel and vertically scanned from the surface of the PDMS membrane by using a motor-driven *XYZ* stage (K701-20RMS, Suruga Seiki) and a stage controller (D73MS, Suruga Seiki). In this paper, we defined the zero-distance (z = 0 μm) as the point where the tip touched on the PDMS membrane surface. The position of the tip touching on the membrane surface can be found clearly from the inverted microscope observation. The scan rate of the probe was set at 5.0 and 20 μm s^{-1} for a single scan and the 2D imaging, respectively.

When the microelectrode tip is located very close to the sample surface, the tip current depends on the distance from the sample surface.[17,38,39] For example, the oxygen reduction current increases when the tip locates near the PDMS or the oxidized PDMS surface because of the higher oxygen-permeability.[39] Whereas the oxygen reduction current decreases near the glass, SU-8, or polystyrene surface due to the negative feedback effect. For the 2D imaging shown in Fig. 3, the minimum distance between the tip and the PDMS membrane surface was set at 20 μm so that the tip current reflects the local oxygen concentration.

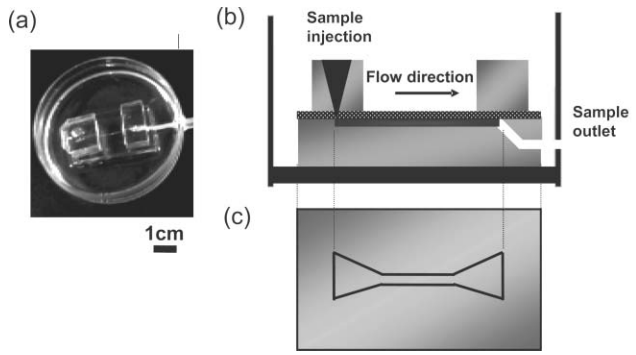

Fig. 1 (a) Photograph and (b) scheme of the PDMS microchannel. Top view of the microchannel design (c).

2.4 Preparation of *E. coli* suspension

Escherichia coli K-12 (IFO3301) stock was provided by the National Collection of Industrial and Marine Bacteria, Ltd (NCIMB), Japan.[21,22] The *E. coli* cells were cultured on a nutrient agar medium (pH 7.2, Nissui Pharmaceutical Co., Ltd, Japan) for more than 12 h at 36.0 °C in an incubator. Colonies from this agar plate were then transferred to a new agar plate with the same components and cultured for 12–15 h at 36.0 °C. The nutrient agar plate comprises 5.0 g L^{-1} beef extract, 10.0 g L^{-1} peptone, 5.0 g L^{-1} NaCl and 15.0 g L^{-1} agar in distilled water. After the second culture, the resulting colonies on the agar plate were immediately suspended and diluted to different concentrations in 200 μL of an aqueous solution containing 7.2 mM $Na_2HPO_4{\cdot}12H_2O$, 2.8 mM KH_2PO_4, 150 mM NaCl, and 100 mM D-(+)-glucose (pH 7.0). The concentration of *E. coli* were accurately determined by using a hemocytometer. The dead *E. coli* suspension was prepared by heating at 70 °C for 30 min.

2.5 Analysis of mass transfer rates in PDMS and SU-8 microchannels

The oxygen reduction current profile measured by SECM was converted to the local oxygen concentration by normalizing to the current in the bulk solution.[21] The oxygen flux (f_z [mol cm^{-2} s^{-1}]) was estimated from Fick's law;

$$f_z = D\,(\Delta C/\Delta z) \quad (1)$$

where D is the diffusion coefficient of oxygen, 2.10 × 10^{-5} cm^2 s^{-1} at room temperature in an aqueous solution.[21] The z-axis is defined as the vertical direction from the center of the microchannel surface. The total mass transfer rates for oxygen between the microchannel and the surrounding PBS solution can be estimated by multiplying the local flux and the small element of area.[21,25,29] In the present system, the shape of the diffusion layer near the microchannel is hemicylindrical (Fig. 2), whereas in the previous study for the spherical cellular masses, an ideal spherical diffusion layer is formed near the very small reaction zone with micrometer dimensions.[21,25,29]

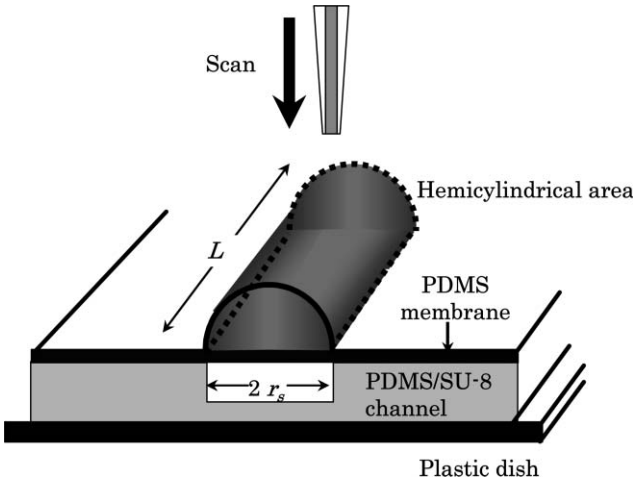

Fig. 2 Schematic illustration of the SECM measurements for the PDMS or SU-8 microchannels. The hemicylindrical area indicates the diffusion layer spread along the microchannel.

The hemicylindrical diffusion area (S_z) and the total mass transfer rates of oxygen (F_z) crossing the diffusion area can be expressed as follows;

$$S_z = \pi z \times L \quad (2)$$

$$F_z = S_z \times f_z \quad (3)$$

where L is the microchannel length (15 000 μm) and z is the radius of the hemicylindrical diffusion layer. Under steady-state conditions, F_z should be constant in any hemicylindrical diffusion layer for certain z and S_z values, and the local flux ($f_z(z)$) and concentration profile ($C(z)$) of oxygen should be linear to $1/z$ and ln z, respectively. However, as the concentration profile near the microchannel (less than half of the microchannel width from the microchannel surface;

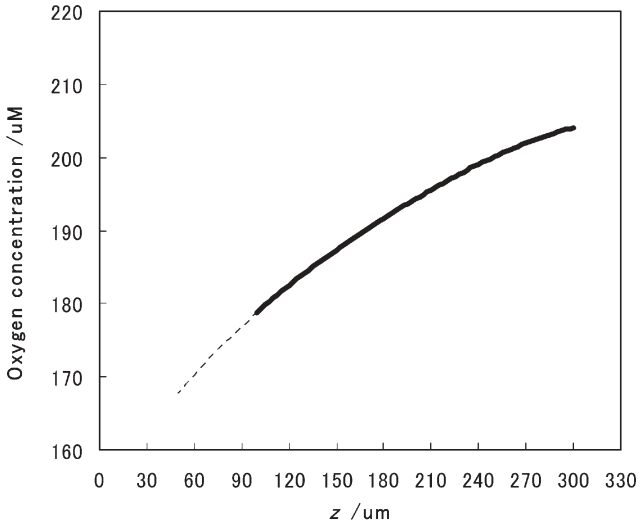

Fig. 4 The oxygen concentration profile as a function of the distance (z) from the PDMS membrane taken at the center of the PDMS microchannel filled with Na_2SO_3. Tip scan rate, 5 μm s^{-1}. Bold line indicates a logarithmic least-square fitting; $y = 23.8 \ln(z) + 68.3$ ($R^2 = 0.999$) ($z = r_s > 100$ μm).

$z < 100$ μm) is not ideally hemicylindrical, logarithm fitting of $C(z)$ was performed for a z range larger than half of the microchannel width ($z > 100$ μm). The fitting of the ln $C(z)$ *vs.* z plot is shown in Fig. 4 ($z > 100$ μm). The correlation coefficient (R) for the plot was almost 1 ($R^2 = 0.999$). Whereas the R^2 value decreased ($R^2 = 0.972$) for the same plot from the smaller distance ($z > 20$ μm).

Diffusion and concentration profile behaviors for cylindrical and microband electrodes have been thoroughly investigated by several research groups.[32–35,38] According to the literature, the current for the microband electrode at a longer time scale depends on the inverse of the logarithm of time, making it impossible to obtain the exact steady-state behavior under

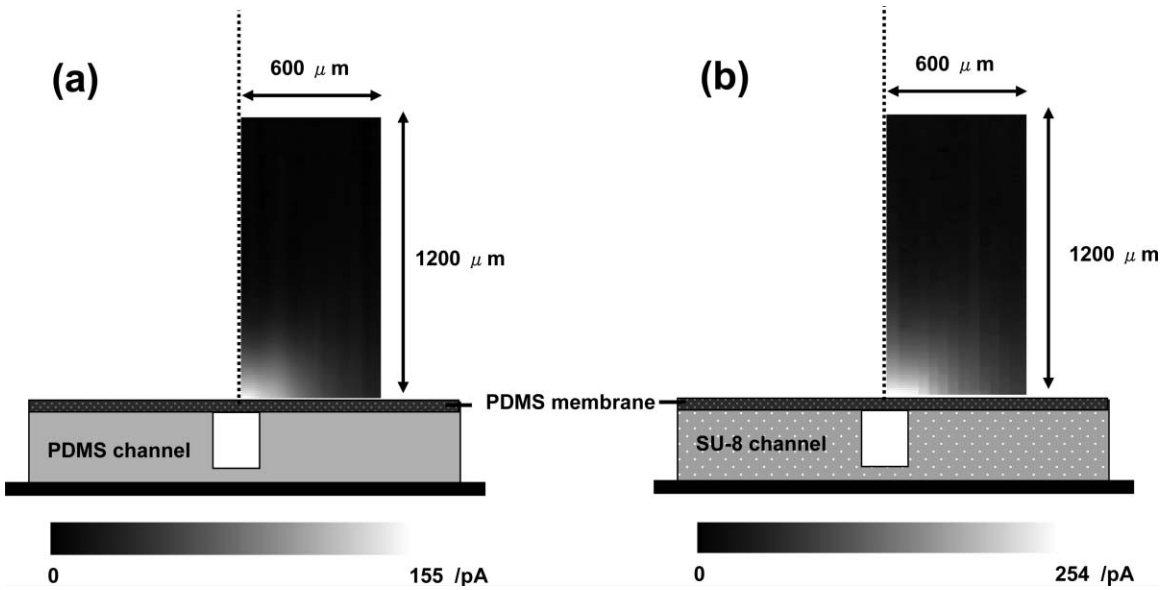

Fig. 3 SECM images monitoring oxygen reduction current profiles around the (a) PDMS and (b) SU-8 microchannels filled with Na_2SO_3. Tip scan rate, 20 μm s^{-1}.

diffusion controlled conditions.[35] However, limiting-like currents are observed experimentally with cyclic voltammetry and chronoamperometry at a relatively longer time scale.[32–35,38] In the time scale of our experimental system (30–60 min), the deviation for the flux expected from the theoretical result[32] is less than 10%, and a deviation from the steady-state concentration profile was not observed during the SECM measurements. This is reasonable because the diffusion layer $(\pi Dt)^{0.5}$ can not growth above several millimeters due to the influence of natural convection.[38]

Fig. 2 shows a schematic illustration of the SECM measurements for the PDMS and SU-8 microchannels. For the PDMS microchannel, the hemicylindrical diffusion area S_z covers the flux in the aqueous phase on the PDMS membrane and includes the oxygen mass transfer to be provided from the PDMS channel phase. On the contrary, for the SU-8 microchannel, S_z covers the entire flux existing in the microchannel because the oxygen permeability of the SU-8 material is very low. Thus, by using the SU-8 microchannel, the real oxygen mass transfer in the microchannel can be evaluated for a comparison with the oxygen flux of the PDMS channel. Since it is difficult to measure the oxygen concentration in the PDMS phase, we have to experimentally compare the total mass transfer rates crossing the S_z area for the PDMS (F_z^{PDMS}) and SU-8 ($F_z^{\mathrm{SU\text{-}8}}$) microchannels. The total oxygen mass transfer rates for the microchannel (F^{total}) can be expressed as follows;

$$F^{\mathrm{total}} = A^{\mathrm{corr}} \times F_z \qquad (4)$$

where A^{corr} is the correction factor and experimentally given as $F_z^{\mathrm{SU\text{-}8}}/F_z^{\mathrm{PDMS}}$ for the PDMS microchannel with an oxygen-free solution (1.0 M Na_2SO_3) and is found to be 1.50 (see the following section). For the SU-8 channel, F^{total} is identical to $F_z^{\mathrm{SU\text{-}8}}$ obtained from eqn (3).

3. Results and discussion

3.1 Evaluation of the oxygen concentration profile near the microchannel

The SECM technique was used to evaluate the mass transfer rates in the microfluidic system to visualize the 2D oxygen concentration profiles near the PDMS and SU-8 microchannels filled with Na_2SO_3 solution. Fig. 3 shows the SECM images for the oxygen reduction current profiles around the (a) PDMS and (b) SU-8 microchannels filled with 1.0 M Na_2SO_3. The amount of Na_2SO_3 is sufficient enough to reduce the oxygen dissolved in the channel;[36,40,41] therefore the solution in the channel is conducted to be oxygen-free. The microelectrode scanned across an area of 1200 μm × 600 μm above the surface of the PDMS membrane. The minimum distance between the tip and the PDMS membrane surface was set at 20 μm. For each image, a bright area with a lower oxygen reduction current was formed near the microchannel because the oxygen was consumed by the chemical reaction of Na_2SO_3 in the microchannel. Thus, these SECM images suggest that the diffusion layer (oxygen depletion region) formed along the microchannel is in a steady-state and is hemicylindrical in shape. It should be noted the current change for the SU-8 channel is greater than that for the PDMS channel. Since PDMS is highly oxygen permeable, the oxygen depletion region is found above the PDMS phase near the PDMS microchannel as well as in the aqueous phase on the channel. On the contrary, for the SU-8 microchannel, the oxygen concentration profiles are formed only in the aqueous solution above the channel.

Fig. 4 shows the plot of the oxygen concentration as a function of the distance (z) from the surface of the PDMS membrane on the PDMS microchannel filled with 1.0 M Na_2SO_3. The oxygen concentration gradually decreased as the tip approached the PDMS surface. The $C(z)$ was numerically fitted with a logarithmic least-square curve for z larger than 100 μm (half of the microchannel width) as shown with a bold line in Fig. 4 ($R^2 = 0.999$). The total oxygen mass transfer rate (F_z^{PDMS}) crossing S_z was determined from eqn (3) as $(2.68 \pm 1.05) \times 10^{-12}$ mol s^{-1} ($n = 15$). Similarly, for the SU-8 microchannel filled with 1.0 M Na_2SO_3, $F_z^{\mathrm{SU\text{-}8}}$ was obtained as $(4.01 \pm 0.30) \times 10^{-12}$ mol s^{-1} ($n = 11$) from these results. From eqn (4), we determined the correction factor ($A^{\mathrm{corr}} = F_z^{\mathrm{SU\text{-}8}}/F_z^{\mathrm{PDMS}}$; see section 2.5) as 1.50, which is useful for estimating the total mass transfer rates of oxygen (F^{total}) for the PDMS microchannel.

We now discuss the maximum oxygen flux through the PDMS membrane by using the SU-8 microchannel device. Since SU-8 is practically impermeable to oxygen, the total oxygen inflow from the air-saturated water phase to the channel was performed through the PDMS membrane on the channel. The apparent maximum oxygen flux for the 7 μm thick PDMS membrane can be obtained by dividing $F_z^{\mathrm{SU\text{-}8}}$ by the effective surface area (200 × 15 000 μm^2) of the PDMS membrane; it was found to be $(1.34 \pm 0.10) \times 10^{-10}$ mol cm^{-2} s^{-1}. This value can be compared with the oxygen mass transfer rates at water–PDMS interfaces;[39] these values are smaller than 2.00×10^{-7} mol cm^{-2} s^{-1} for the water–plain PDMS interface and 8.00×10^{-9} mol cm^{-2} s^{-1} for the water–oxygen-plasma treated PDMS interface. Thus, the apparent oxygen flux obtained here by using the SU-8 device is sufficiently smaller than the values for the water–PDMS interfaces. These results suggest that the rate-determining step for the oxygen inflow is the mass transfer in the aqueous phase and/or that in the channel. Since the PDMS membrane is thin (7 μm) and the oxygen transfer at the water–PDMS membrane is rapid, the influence of the mass transfer through the membrane will be negligible in the present device. The design of the microchannel (width, height, or other dimensions, and the materials used), including the membrane thickness, is important to control the oxygen mass transfer rates for such microfluidic devices.

3.2 Biological activity of *Escherichia coli* K-12 in the microchannel

The device was applied for the estimation of the biological activity of *E. coli* cells. Fig. 5 shows the oxygen concentration profile above the microchannel filled with an *E. coli* suspension of alive or dead cells (2.83×10^{11} cells ml^{-1} for each). A significant decrease in the localized oxygen concentration is observed near the microchannel filled with the alive *E. coli*

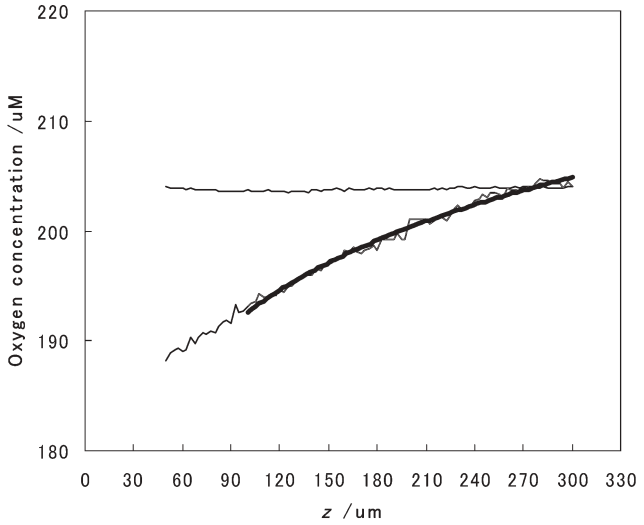

Fig. 5 The oxygen concentration profile for a PDMS microchannel filled with an *E. coli* suspension of alive or dead cells. Bold line indicates a logarithmic least-square fitting; (y = 11.2 ln(z) + 141.0 (R^2 = 0.987) ($z = r_s > 100$ μm).

suspension, whereas the change in oxygen concentration is almost negligible for the dead cells. The oxygen consumption rates of the alive *E. coli* (F^{total}) were estimated by using logarithmic least-square methods, and were found to be 1.66×10^{-12} mol s^{-1} (R^2 = 0.987). The F^{total} value depends on the number of *E. coli* cells (N) in the microchannel as shown in Fig. 6(a). The F^{total} almost linearly increased with the logarithm of the concentration of *E. coli* cells ($10^6 \sim 10^8$ cells). The oxygen consumption rate of a single *E. coli* cell (F^{total}/N) was found to be $\sim 4.31 \times 10^{-20}$ mol s^{-1} cell^{-1} (Fig. 6(b)). This value is lower by one order of magnitude than the value, 4.40×10^{-19} mol s^{-1} cell^{-1}, reported by Kaya *et al.* for *E. coli* embedded in collagen gel within a 1.80 nL volume microwell.[21] This discrepancy suggests that environmental conditions will also affect cellular respiration activity. Further investigation is required to adjust the design of the microchannel device, such as width, height, and length of the microchannel or even the material (PDMS, SU-8, and others) of the microchannel device. The measurement and analysis procedure introduced in the present study will be widely applicable for biological microfluidic devices with channel-like reaction zones.

4. Conclusions

The oxygen concentration profile near the PDMS membrane on a microchannel filled with Na_2SO_3 or *E. coli* was determined by SECM. The total oxygen mass transfer rates to the PDMS membrane (F^{total}) were quantitatively evaluated using the hemicylindrical diffusion model expanded on the microchannel. This microchannel device combined with the SECM technique will be widely applicable to evaluate the respiratory activity of *E. coli* suspensions: the oxygen consumption by a single *E. coli* cell was found to be $\sim 4.31 \times 10^{-20}$ mol s^{-1} cell^{-1}. The significant advantages of this device over conventional systems are the capability for continuous measurement and a sample volume as small as several

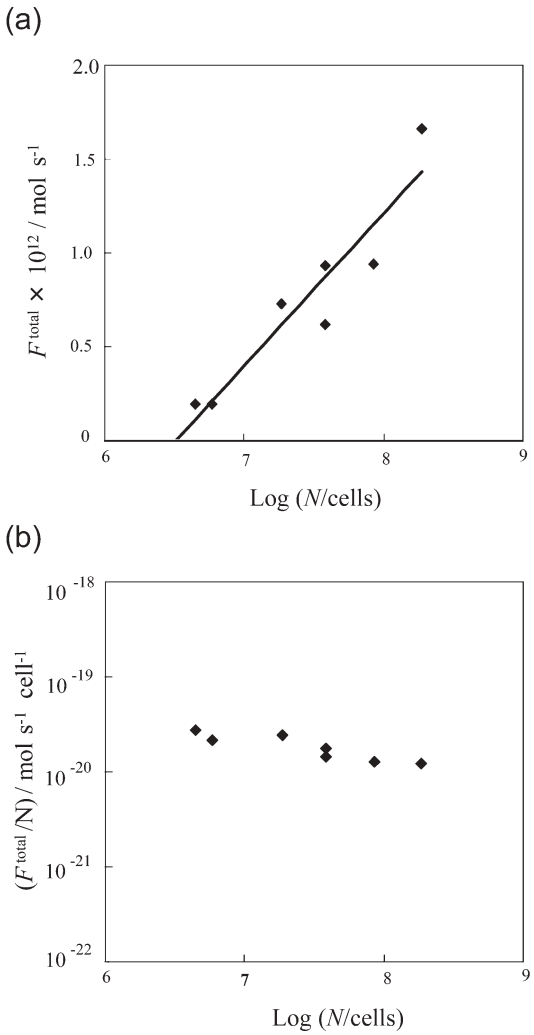

Fig. 6 (a) The *E. coli* respiratory activity (F^{total}) in a microchannel and (b) the *E. coli* respiratory activity by a single cell (F^{total}/N)) as a function of cell number (N).

nanolitres. These devices will be widely applicable to evaluate the metabolism of biological samples.

Acknowledgements

This work was partly supported by a research project for utilizing advanced technologies in agriculture, forestry and fisheries, established by the Ministry of Agriculture, Forestry and Fisheries of Japan, the R&D Program for Environmental Nanotechnology from National Institute for Environmental Studies and Grants-in-Aid for Scientific Research (No. 17710112 and 18101006) from the Ministry of Education, Science and Culture, Japan.

References

1 D. Qin, Y. N. Xia, J. A. Rogers, R. J. Jackman, X. M. Zhao and G. M. Whitesides, *Microsystem Technology in Chemistry and Life Science Topics in Current Chemistry*, Springer, Germany, 1998, vol. 194, ch. 2, pp. 1–20.
2 D. Qin, Y. N. Xia and G. M. Whitesides, *Adv. Mater.*, 1996, **8**, 917–919.

3 M. M. Stevens, M. Mayer, D. G. Anderson, D. B. Weibed, G. M. Whitesides and R. Langer, *Biomaterials*, 2005, **26**, 7636–7641.
4 V. Studer, R. Jameson, E. Pellereau, A. Pepin and Y. Chen, *Microelectron. Eng.*, 2004, **73–74**, 852–857.
5 E. Leclerc, K. S. Furukawa, F. Miyata, Y. Sakai, T. Ushida and T. Fujii, *Biomaterials*, 2004, **25**, 4683–4690.
6 R. S. Suh, X. Zhu, N. Phadke, D. A. Ohl and S. Takayama, *Hum. Reprod.*, 2005, **30**, 1–7.
7 J. H. Wittig, A. F. Ryan and P. M. Asbeck, *J. Neurosci. Methods*, 2005, **144**, 79–89.
8 D. J. Beebe, M. B. Wheeler, H. Zeringue, E. M. Walters and S. Raty, *Theriogenology*, 2002, **57**, 125–135.
9 S. Raty, E. M. Walters, J. Davis, H. Zeringue, D. J. Beebe, S. L. Rodriguez-Zas and M. B. Wheeler, *Lab Chip*, 2004, **4**, 186–190.
10 W. DiLuzio, L. Turner, M. Mayer, P. Garstecki, D. B. Weibel, H. C. Berg and G. M. Whitesides, *Nature*, 2005, **435**, 1271–1274.
11 B. S. Cho, T. G. Schuster, X. Zhu, D. Chang, G. D. Smith and S. Takayama, *Anal. Chem.*, 2003, **75**, 1671–1675.
12 K. M. Horsman, S. L. Barker, J. P. Ferrance, K. A. Forrest, K. A. Koen and J. P. Landers, *Anal. Chem.*, 2005, **77**, 742–749.
13 S. Takayama, J. C. McDonald, E. Ostuni, M. N. Liang, P. J. A. Kenis, R. F. Ismagilov and G. M. Whitesides, *Proc. Natl. Acad. Sci. U. S. A.*, 1999, **96**, 5545–5548.
14 N. Szita, P. Boccazzi, Z. Y. Zhang, P. Boyle, A. J. Sinskey and K. F. Jensen, *Lab Chip*, 2005, **5**, 819–826.
15 A. Zanzotto, N. Szita, P. Boccazzi, P. Lessard, A. J. Sinskey and K. F. Jensen, *Biotechnol. Bioeng.*, 2004, **87**, 243–254.
16 G. Wittstock, *Fresenius' J. Anal. Chem.*, 2001, **370**, 303–315.
17 M. Gonsalves, A. L. Barker, J. V. Macpherson, P. R. Unwin, D. O'Hare and C. P. Winlove, *Biophys. J.*, 2000, **78**, 1578–1588.
18 S. Isik, M. Etienne, J. Oni, A. Blochl, S. Reiter and W. Schuhmann, *Anal. Chem.*, 2004, **76**, 6389–6394.
19 B. Liu, W. Cheng, S. A. Rotenberg and M. V. Mirkin, *J. Electroanal. Chem.*, 2001, **500**, 590–597.
20 T. Yasukawa, I. Uchida and T. Matsue, *Biophys. J.*, 1999, **76**, 1129–1135.
21 T. Kaya, D. Numai, K. Nagamine, S. Aoyagi, H. Shiku and T. Matsue, *Analyst*, 2004, **129**, 529–534.
22 K. Nagamine, T. Kaya, T. Yasukawa, H. Shiku and T. Matsue, *Sens. Actuators, B*, 2005, **108**, 676–682.
23 H. Shiku, Y. Torisawa, A. Takagi, S. Aoyagi, H. Abe, H. Hoshi, T. Yasukawa and T. Matsue, *Sens. Actuators, B*, 2005, **108**, 597–602.
24 K. Takoh, A. Takahashi, T. Matsue and M. Nishizawa, *Anal. Chim. Acta*, 2004, **522**, 45–49.
25 Y. Torisawa, H. Shiku, T. Yasukawa, M. Nishizawa and T. Matsue, *Sens. Actuators, B*, 2005, **108**, 654–659.
26 Y. Torisawa, H. Shiku, T. Yasukawa, M. Nishizawa and T. Matsue, *Biomaterials*, 2005, **26**, 2165–2172.
27 B. Agung, T. Otoi, H. Abe, H. Hoshi, M. Murakami, N. W. Karja, M. K. Murakami, P. Wongsrikeao, H. Watari and T. Suzuki, *Reprod. Domest. Anim.*, 2005, **40**, 51–56.
28 A. S. Lopes, L. H. Larsen, N. Ramsing, P. Lovendahl, M. Raty, J. Peippo, T. Greve and H. Callesen, *Reproduction*, 2005, **130**, 669–679.
29 H. Shiku, T. Shiraishi, S. Aoyagi, Y. Utsumi, M. Matsudaira, H. Abe, H. Hoshi, S. Kasai, H. Ohya and T. Matsue, *Anal. Chim. Acta*, 2004, **522**, 51–58.
30 H. Shiku, T. Shiraishi, H. Ohya, T. Matsue, H. Abe, H. Hoshi and M. Kobayashi, *Anal. Chem.*, 2001, **73**, 3751–3758.
31 S. Toshima, T. Kanbayashi, K. Kan, K. Aoyagi and M. Kobayashi, *Electrochemistry*, 2005, **73**, 942–944.
32 K. Aoki, K. Tokuda and H. Matsuda, *J. Electroanal. Chem.*, 1987, **230**, 61–67.
33 S. Coen, D. K. Gallo and D. E. Tallman, *J. Electroanal. Chem.*, 1986, **215**, 29–48.
34 M. R. Deakin, R. M. Wightman and C. A. Amatore, *J. Electroanal. Chem.*, 1986, **215**, 49–61.
35 P. M. Kovach, W. L. Caudill, D. G. Peters and R. M. Wightman, *J. Electroanal. Chem.*, 1985, **185**, 285–295.
36 C.-C. Wu, T. Yasukawa, H. Shiku and T. Matsue, *Sens. Actuators, B*, 2005, **110**, 342–249.
37 T. Matsue, N. S. Koike and I. Uchida, *Biochem. Biophys. Res. Commun.*, 1993, **197**, 1283–1287.
38 C. Combellas, A. Fuchs and F. Kanoufi, *Anal. Chem.*, 2004, **76**, 3612–3618.
39 H. Shiku, T. Saito, C.-C. Wu, T. Yasukawa, M. Yokoo, H. Abe, T. Matsue and H. Yamada, *Chem. Lett.*, 2006, **35**, 234–235.
40 E. Gasana, P. Westbroek, E. Temmerman, H. P. Thun and F. Twagiramungu, *Electrochem. Commun.*, 2000, **2**, 727–732.
41 L. Genies, Y. Bultel, R. Faure and R. Durand, *Electrochim. Acta*, 2003, **48**, 3879–3890.